A Computational Model for Heat Transfer Coefficient Estimation in Electric Arc Furnace

Vito Logar,* Amirhossein Fathi, and Igor Škrjanc

The paper studies the effects of solid and liquid steel properties on the heat transfer coefficient (HTC) in electric arc furnaces (EAFs). Mathematically speaking, the HTC is a function of solid and liquid steel properties. Different velocities of the bath cause different flow paths around the solid particles and therefore different HTCs—a computational issue that has not been addressed yet. Therefore, a simplified calculation model is proposed, intended for HTC estimation according to the EAF conditions. Although many studies investigated this topic, most of them either assume unconventional conditions for the EAF operation, are computationally complex or focus on a specific case; and are, therefore, hard to implement in general EAF models. The algorithm proposed in this paper introduces simplified, yet accurate equations for calculating the HTC between solid and liquid steels as a function of their properties. Due to simplicity of the algorithm, the computational times are very short; thus, the procedure can be used in online model environments in order to perform different heat-transfer-related calculations. The obtained results show high similarity with other practical and theoretical studies. Furthermore, implementation of the HTC calculation submodule in a comprehensive EAF model yielded high accuracy in steel-bath temperature prediction.

1. Introduction

Electric arc furnaces (EAFs) are becoming more and more enhanced and optimized when it comes to tap-to-tap times and energy consumptions. Tap-to-tap times have been shortened to approximately 30–40 min per batch for a 100–130 ton EAF, loaded with only one scrap basket.[1] The share of the steel, produced by the EAFs has increased from 16.9% in 1975[2] to 29.2% in 2011[3] and is expected to grow for another 50% in the next 20–30 years.[4] New technologies on EAF process optimization are evolving, including software algorithms for smart sensing, simulation and model-based control, which are all based on process models of any kind. In the search for the best EAF model, each aspect of the steel-melting process should be taken into the account if possible. Since melting of the scrap is closely related to the overall energy balance and energy consumption of the EAF, a computational model of the melting, and the related processes represents one of the more important submodels. EAF models, designed for simulation, control or production planning, require a heat-transfer coefficient (HTC) calculation submodule that determines the HTC between solid and liquid steels and covers a wide range of EAF conditions with low computational complexity.

Although, the HTCs represent one of the more important aspects in thermal modeling, the knowledge on the actual HTC values for different EAF conditions is very limited and hard to acquire. The literature review on simulation/control based models reveals that many of the EAF models use constant HTCs between solid and liquid steels, e.g., Bekker et al.[5] assumed this value to be approximately 400 W $(m^2\,K)^{-1}$ and Logar et al.[6,7] assumed it to be approximately 200 W $(m^2\,K)^{-1}$. The EAFs modeled in these papers were not equipped with stirring; therefore, these values cannot be used for other EAFs with such functionality present.

On the other side, according to the importance of the problem, some papers have studied the effect of the parameters, such as scrap dimensions, bath temperature, and bath velocity,[8] on the melting process. Guthrie and Gourtsoyannis[9] developed a model to calculate the melting time of spherical scrap in non-stirred bath. Using

[*] Prof. V. Logar
Laboratory of Modelling, Simulation and Control, Faculty of Electrical Engineering, University of Ljubljana, Tržaška 25, SI-1000 Ljubljana, Slovenia
Email: vito.logar@fe.uni-lj.si
A. Fathi
Department of Energy Engineering, Sharif University of Technology, Azadi Ave., Tehran, Iran
Prof. I. Škrjanc
Laboratory of Modelling, Simulation and Control, Faculty of Electrical Engineering, University of Ljubljana, Tržaška 25, SI-1000 Ljubljana, Slovenia

DOI: 10.1002/srin.201500060

the laminar natural convection mechanism, which has in this case the highest effect on the melting time, the approximation for the melting time was about 100 s (due to spherical shape of the scrap with 5 in. diameter). The results of the numerical model have been compared to experimental results and due to some simplifications in the model, the model-estimated melting time was larger than experimental melting time. In this study, the HTC was determined by using the Nusselt number as presented in Equation 1:

$$Nu = 0.539\left[Pr\frac{GrPr}{0.952 + Pr}\right]^{\frac{1}{4}}. \quad (1)$$

Kawakami et al.[10] studied heat and mass transfer of scrap melting in a steel bath. Based on experimental results, the numerical model was adjusted and the conclusion of the study revealed that HTC should be in the range from 27.7 to 77.2 kW $(m^2\,K)^{-1}$ The HTC value has been computed for steel bars positioned vertically in molten bath with 180 mm height and different diameters, i.e., 30, 40, and 50 mm. Reverse relation between HTC and scrap radius was shown and finally the Nusselt number (Equation 2) and the Sherwood number (Equation 3) were suggested:

$$Nu = 0.017Re^{0.8}Pr^{0.33}, \quad (2)$$

$$Sh = 0.017Re^{0.8}Sc^{0.33}. \quad (3)$$

Li et al.[11] investigated the effect of different sizes and initial temperatures of the steel bars on their melting time. The melting process has been simulated using a two dimensional phase field model with constant HTC by implementing Equations 4 and 5, where Equation 4 represents the boundary condition and Equation 5 represents the heat conduction inside the solid scrap, respectively:

$$h(T_{lSc} - T_m) = \rho_{sSc}\Delta H_f\vartheta - k_{sSc}\frac{\partial T}{\partial x}\bigg|_{int}, \quad (4)$$

$$\frac{\partial}{\partial x}\left(k_{sSc}\frac{\partial t}{\partial x}\right) = \rho_{sSc}\frac{\partial(C_{P_{sSc}}T)}{\partial t}. \quad (5)$$

The HTC has been estimated by Equations 6 and 7:

$$Nu = \frac{h_{motionless}L_C}{k_{lSc}} = 0.686(Gr.Pr)^{\frac{1}{4}}, \quad (6)$$

$$h = \frac{\rho C_p \upsilon}{e^{h_{motionless}-1}}. \quad (7)$$

The coefficient was predicted at 13.4 kW $(m^2\,K)^{-1}$ in motionless bath at film temperature of 1585 °C. Simulated and experimental data were comparable and the conclusion of the study was that increase of the scrap temperature decreases the melting time linearly.

Shukla et al.[12] designed a model using ice in water vessel equipped with argon injection system as a stirrer in order to replicate the EAF conditions. Dimensionless numbers (*Nu*, *Re*, *Pr*, and *Gr*) have been derived based on the sets of experimental data for different ice geometries. The experimental results showed that the average value of the HTC, considering the shapes, is in the range from 461 to 793 W $(m^2\,K)^{-1}$ with zero argon injection and can reach up to 3223–6110 W $(m^2\,K)^{-1}$at argon injection flow of 100 (N dm^3) h^{-1}, which caused water velocities of approximately 0.3 m s^{-1}.

Arzpeyma et al.[8] studied a cylindrical scrap submerged in the steel bath. The HTC was calculated by estimating the Nusselt number and since the Reynolds number was higher than 10^5, Nusselt number suggested by Kreith[13] was used as shown in Equation 8:

$$Nu = 0.0266Re^{0.805}Pr^{\frac{1}{3}}, 40\,000 \le Re \le 40\,0000. \quad (8)$$

The calculation has been implemented in the EAF model based on continuity equation, momentum conservation equation, turbulence model, melting model, and energy conservation model. The effect of scrap radius, preheating temperature, magnetic force (bath velocity), and stirring direction have been evaluated and the results demonstrated that solid scrap temperature change during the melting is not significant and for this reason the HTC reduces with reducing residual scrap.

The literature review reveals that some useful models of HTC prediction between solid and liquid scrap have been developed; however, many of them are hard to apply in a simulation and/or control based simulation due to numerous reasons. First, some models assume conditions that significantly deviate from the normal EAF operation, such as solid steel density and its placement in the bath, e.g., a steel bar is not expected to be positioned axially in the bath[10,11] and steel scrap diameter is not expected to be constant.[8] Second, a lot of the models include computationally complex problems, usually employing volume of fluid methods or phase field approach, which furthermore requires excellent problem description or the results are not reliable. Third, most of the approaches do not consider bath velocity distribution.

For the above reasons, this paper aims to propose a HTC calculation algorithm, which overcomes the aforementioned flaws, allows its use in broader EAF-model environments and is designed especially for online process monitoring and model-based control applications. To develop and validate the proposed calculations, the algorithm has been implemented as a submodule in the EAF model as shown by **Figure 1**.

The HTC submodule uses six state variables to describe the steel properties and one exogenous variable to describe the bath velocity. The overall EAF model shown in Figure 1 describes the EAF process by 18 inputs, more than 300 algebraic variables, and 71 state variables. During melting, each iron resource or additive charged can be described by

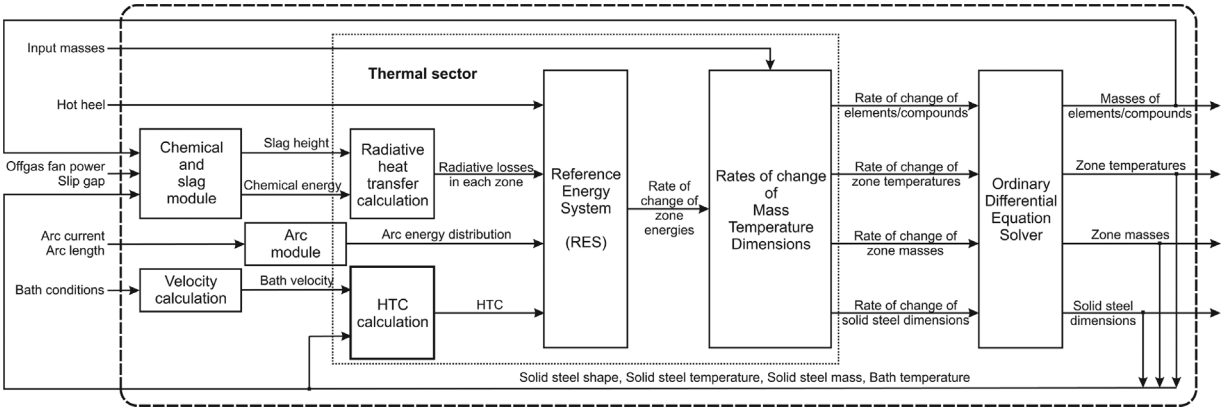

Figure 1. Schematic representation of the EAF model including the proposed HTC calculation.

two state variables, i.e., its mass and temperature, in order to obtain an accurate model to predict the temperatures of the solid and liquid steel. In order to simplify the structure of the model and to decrease the computational load, two state variables describing the HBI/DRI resource are neglected and the charged HBI/DRI is assumed to melt instantaneously. Such an assumption is common in similar studies[5–7] related to this work, as the research has shown that melting time of the HBI/DRI particles is very short in comparison to the tap-to-tap times and can, therefore, be neglected. However, this assumption is true only when adding the HBI/DRI to the steel bath in the amount that is substantially smaller than the total mass of the bath; therefore, neglecting the bath temperature drop due to charged HBI/DRI. Whether the EAF is initially charged with HBI/DRI or the amount of the charged HBI/DRI is large enough the instantaneous melting of the particles does not apply.

2. Modeling

Solid steel in an EAF vessel exchanges thermal energy with bath, arcs, gas burners, walls and also gas in the EAF freeboard. When the amount of the liquid steel is high enough to submerge the solid, the heat transfer between them occurs mainly through convection of the heat. The presented paper focus on this melting stage, where the amount of the heat that is transferred can be evaluated by the Newton's law, which states that the amount of the heat transferred [$Q_{\mathrm{lSc-sSc}}$] is dependent on temperature difference between the liquid and the solid steel ($T_{\mathrm{lSc}} - T_{\mathrm{sSc}}$), the area over which the heat transfer takes place (A) and the HTC (h). Equation 9 represents the Newton's law:

$$Q_{\mathrm{lSc-sSc}} = hA(T_{\mathrm{lSc}} - T_{\mathrm{sSc}}). \tag{9}$$

The HTC depends on many factors, such as liquid and solid steel properties, temperatures, velocity of the steel bath, dimensions, shape of the interface, etc. These factors affect the parameters, which can be categorized into two groups, i.e., solid steel properties and steel bath properties.

The properties related to solid steel, charged either as HBI/DRI or scrap, are its temperature, density, shape, and dimensions. The HBI/DRI shapes, sizes, and densities are specified for nearly all producers.[14,15] On the other side, steel scrap covers a wider range of densities, dimensions, and shapes[14] and due to notable melting time, both bath and scrap temperatures change during the melting.

In order to find the temperature and mass change of the scrap, heating and melting rate coefficients can be used to avoid solving of the partial differential equations. Those coefficients are estimated according to the melting stage. When a solid particle is submerged into the bath, it experiences three stages of melting until it completely melts. First, a frozen shell is formed around the particle. Second, due to diffusing carbon dissolved in the liquid steel, melting temperature of the solid is reduced. And finally, the solid particle melts rapidly due to the high melting rate.[16] In the solidification stage, the energy exchanged is assumed to cause the increase in the temperature of the particle. The formation of the frozen shell around it continues until its conductivity becomes lower than the conductivity of the molten steel. Therefore, the heating and melting rate coefficients are normally a function of bath and scrap temperature, i.e., $\frac{T_{\mathrm{sSc}}}{T_{\mathrm{lSc}}}$ and $1 - \frac{T_{\mathrm{sSc}}}{T_{\mathrm{lSc}}}$ for melting and heating rate, respectively,[5–7] or $\sqrt{\frac{T_{\mathrm{sSc}}}{T_{\mathrm{lSc}}}}$ and $1 - \sqrt{\frac{T_{\mathrm{sSc}}}{T_{\mathrm{lSc}}}}$ for melting and heating rate, respectively.[17] The rate of change of temperature and mass are presented using Equations 10 and 11,[6,7] where melting and heating rate coefficients are utilized as $\frac{T_{\mathrm{sSc}}}{T_{\mathrm{lSc}}}$ and $\left(1 - \frac{T_{\mathrm{sSc}}}{T_{\mathrm{lSc}}}\right)$, respectively:

$$\frac{dT_{\mathrm{sSc}}}{dt} = \frac{Q_{\mathrm{sSc}}\left(1 - \frac{T_{\mathrm{sSc}}}{T_{\mathrm{lSc}}}\right)}{m_{\mathrm{sSc}} C_{\mathrm{p_{sSc}}}(T_{\mathrm{sSc}})}, \tag{10}$$

$$\frac{dm_{\mathrm{sSc}}}{dt} = \frac{Q_{\mathrm{sSc}} \frac{T_{\mathrm{sSc}}}{T_{\mathrm{lSc}}}}{\int_{T_{\mathrm{m}}}^{T_{\mathrm{lSc}}} C_{\mathrm{plSc}}(T) d_{\mathrm{T}} + \Delta H_{\mathrm{f}} + \int_{T_{\mathrm{sSc}}}^{T_{\mathrm{m}}} C_{\mathrm{psSc}}(T) d_{\mathrm{T}}}. \tag{11}$$

The properties related to the steel bath are bath velocity and temperature. Bath velocity and its distribution is a function of CO formation, electromagnetic forces, shear stress, natural convection, and stirring.[16] The velocity distribution and direction depends on the amount, size, and position of the scrap in the bath. As Paik and Nguyen[18] and Gonzalez et al.[19] have shown that the velocity field in the bath affected by the buoyancy force includes two different circulating loops when the complete zone is filled by liquid metal and there is no slag formation on top of the bath. One of them points in clockwise and the other in counterclockwise direction as shown in **Figure 2**. According to the study, it is assumed that two different bath flows around the scrap can occur, depending whether the scrap is located in the center or more to the edge of the vessel. Furthermore, it is assumed that the solid steel is completely submerged in the steel bath.

According to the literature review, two common methods to compute the HTC are used. The first is to estimate the HTC in motionless bath and then use Equation 7 to adapt it.[11,12] In this manner, Nusselt number is a function of Grashof and Prandtl numbers.[12] The second method considers forced convection, where the Nusselt number is as a function of Reynolds and Prandtl numbers.[12] A large range of Nusselt number equations has been developed for this case, with Prandtl and Reynolds numbers powered to $\frac{1}{3}$ and $\frac{1}{2}$, respectively, e.g., the Nusselt number proposed by Shukla et al.[12] uses Prandtl and Reynolds numbers with such powers. Most calculations[8,20] already implicitly involve the bath flow path; therefore, equation coefficients are modified in comparison to the coefficients in the original equations.

The Nusselt number proposed in this study assumes a cubic shape of the scrap, i.e., calculations are based on the cuboid model. The reasons for this assumption are the following: first, the cuboid model is physically suitable for the given problem; second, Reynolds and Prandtl number powers are similar to other studies; and finally, the effect of the characteristic length of the cuboid and the flow path/direction are taken into the account in HTC calculation. In cuboid model, the Nusselt number based on the characteristic length can be described by Equation 12[21] and the characteristic length of the cuboid can be represented by Equation 13:[21,22]

$$Nu = \frac{2}{\sqrt{\pi}} \frac{1}{\sqrt{\frac{L_P C_{BLP}}{RePr^{\frac{1}{3}} L_C}}}, \tag{12}$$

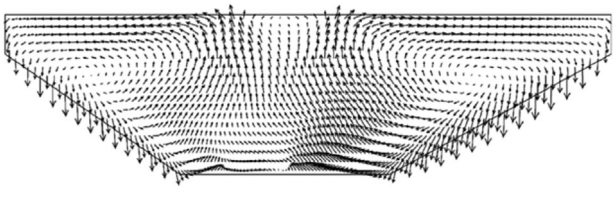

Figure 2. Cross-sectional view of the velocity field in an AC-EAF.[19]

$$L_C = \sqrt{2(HL + WL + HW)}, H \le W \le L, \tag{13}$$

where L_P is the length of the flow path, obtained according to the solid steel position in the bath, Pr is the Prandtl number obtained by Equation 15, Re is the Reynolds number obtained by Equation 16, C_{BPL} is boundary layer parameter $\frac{U_\infty}{u_e}$, where u_e is the linearized effective velocity obtained by linearization of the laminar boundary layer momentum equation. Based on the available solution methods and conditions, C_{BLP} is predicted between 2.13 and 2.77[21]

$$Pr = \frac{C_p \mu}{K}, \tag{15}$$

$$Re = \frac{V_{lSc} \rho L_C}{\mu}. \tag{16}$$

By knowing the Nusselt number, the HTC can be calculated by Equation 17:

$$h = \frac{NuK}{L_C}. \tag{17}$$

Physical properties, such as specific heat capacity, thermal conductivity, density and dynamic viscosity are considered at film temperature, which is the average value of the combined solid and bath temperatures. Furthermore, melting of solid parts reduces their dimensions equivalently.

Due to time-variant conditions in the EAF during the melting process, the HTC changes continuously. In order to simplify the model and the corresponding calculations, but maintain the effect of varying conditions on the HTC, an average HTC can be calculated for the given melting time. In this study, Equation 18 is used to obtain the average HTC:

$$\bar{h} = \frac{\int_0^{Ti_{melting}} h(A(t), T_{lSc}(t), V_{lSc}(t), T_{sSc}(t)) A(t) (T_{lSc}(t) - T_{sSc}(t)) d_t}{\int_0^{T_{melting}} A(t)(T_{lSc}(t) - T_{sSc}(t)) d_t}. \tag{18}$$

The HTC calculated by Equation 18 assumes that bath temperature, bath velocity, scrap density and scrap dimensions are known.

3. Results

The effect of solid and liquid steel properties on the average HTC is studied for two different cases, i.e., first, when the scrap is placed in the center; and second, when the scrap is placed at the edges of the EAF vessel. Furthermore, the effect of the bath temperature and scrap density on the average HTC and melting time are

investigated. The presented results are valid for the case when the steel scrap is completely submerged in the bath. The results have shown that bath temperature and scrap density affect the melting time of the scrap; however, they do not affect the average HTC. Finally, general equations for estimation of the average HTC and melting time of the solid steel submerged in the steel bath are presented. All presented equations are valid for solid steel at 298 K initial temperature, bath velocities between 0.005 $\frac{m}{s}$ and 0.5 $\frac{m}{s}$ and steel cubes with the side ($L = W = H = L_{sSc_0}$) between 0.2and 1.0 m. The reason to propose the equations for cubic-shaped and not cuboid-shaped scrap is twofold; first, the HTC calculation becomes a function of two instead of four input variables; and second, using a combination of different cubic shapes, an HTC calculation of many typical steel shapes, e.g., bars, can be obtained.

First, the effect of bath temperature change on average HTC was calculated. For this reason, the average HTC was computed at two different bath temperatures, i.e., 1800 and 1900 K, respectively. The study revealed that the increase in the average HTC when bath temperature is increased from 1800 to 1900 K is approximately 0.5% and can therefore be neglected. Furthermore, the study has shown that scrap density does affect the scrap melting time, but does not affect the average HTC.

Second, the effect of the bath temperature on the scrap melting time is investigated. The results as presented in **Figure 3** show that increasing the bath temperature shortens the melting time linearly.

Since the decrease of the melting time (DMT) is linear it can be described by Equation 19 as a function of bath temperature:

$$DMT = 0.07556(T_{lSc} - 1800)\%, \quad \begin{matrix} 1800\text{K} \le T_{lSc} \le 1900\text{K} \\ T_{sSc_0} = 298\text{K} \end{matrix} \tag{19}$$

Finally, the effect of scrap size, bath velocity and scrap position in the bath are presented. Since the steel density does not affect the average HTC, but only the melting time (the relation between the melting time and scrap density is linear), the calculation of the average HTC ($\bar{h}_{scrap}$) and the melting time ($Ti_{melting}$) can be performed using Equations 20 and 21. The average HTC calculation as presented by Equation 20 is a function of scrap location in the bath (C_{SL}), bath velocity (V_{lSc}) and scrap size at initial conditions (L_{sSc_0}). The average melting time calculation as presented by Equation 21 is a function of scrap density (ρ_{sSc}), bath velocity (V_{lSc}) and scrap size (L_{sSc_0}). These are obtained by the following procedure. First, the average HTC is calculated for each condition using Equations 9–18. Afterward, a surface fitting technique is used to find general mathematical equations to describe the average HTC and melting time as a function of solid and liquid steel specifications.

$$\bar{h}_{scrap} = 9890 C_{SL} V_{lSc}^{0.5} . L_{sSc_0}^{-0.5}, \quad \begin{matrix} 0.005\frac{m}{s} \le V_{lSc} \le 0.5\frac{m}{s} \\ 0.2\text{m} \le L_{sSc_0} \le 1.0\text{m} \end{matrix} \tag{20}$$

$$t_{Melting} = \left[\frac{156.2}{C_{SL}} V_{lSc}^{-0.5} L_{sSc_0}^{1.5}\right]\left(\frac{\rho_{sSc}}{3000}\right), \quad \begin{matrix} 0.005\frac{m}{s} \le V_{lSc} \le 0.5\frac{m}{s} \\ 0.2\text{m} \le L_{sSc} \le 1.0\text{m} \end{matrix} \tag{21}$$

where L_{sSc_0} is the scrap cube size ($L = W = H = L_{sSc_0}$) at the beginning of the melting, ρ_{sSc} is the scrap density and C_{SL} is the coefficient representing the effect of the scrap placement in the bath. The value of C_{SL} is 1 when the scrap is placed at the edge of the vessel and $\frac{4}{3}$ when the scrap in placed in the center of the vessel.

Equation 20 represents the reverse relation between the HTC and the scrap area submerged in the bath, e.g., $\bar{h}_{HBI} \equiv \frac{1}{A}$ (where A is the scrap area submerged in the bath). The results have shown that bath velocity has a direct relation with the HTC as concluded by other similar studies.[11,12]

Using Equation 20, **Figure 4** is obtained, showing the average HTC in relation to bath velocity and scrap size for both cases, i.e., scrap placement at the edge (a) and in the center (b) of the vessel.

As can be seen in Figure 4, the HTC increases, when the scrap dimensions decrease or the bath velocity increases.

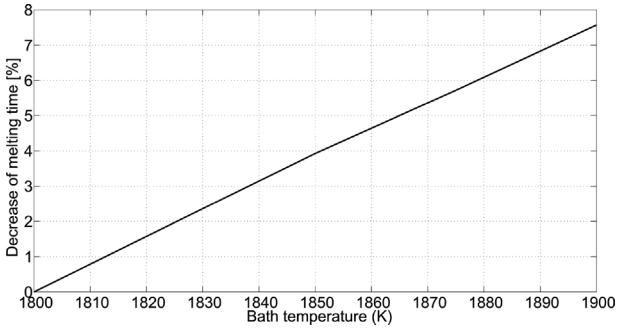

Figure 3. The effect of the bath temperature on the melting time.

4. Validation

Up to now, some studies have been performed to predict the HTC between solid and liquid steels. All mathematical models that were developed are computationally complex; however, the results are usually limited to a special case, with many unconventional assumptions about the EAF conditions. Therefore, the proposed model tries to resolve those challenges, i.e., to reduce the calculation time, preserve the accuracy of the estimation, and to generalize the approach to be useful for different sizes of the solid steel and bath velocities. The model presented in this work

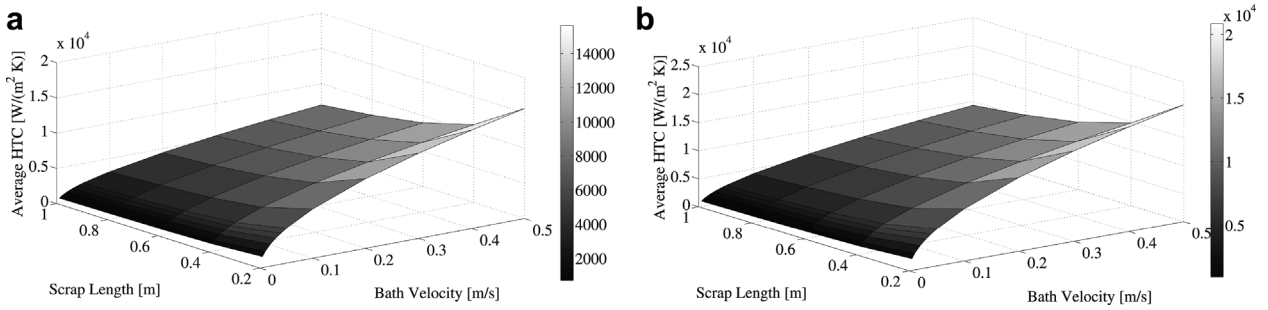

Figure 4. The average HTC in relation to bath velocity and scrap size for scrap located at the edges a) and in the center b) of an EAF.

is validated using assumptions, results and conclusions of the studies in the literature review in order to show the accuracy of the proposed algorithm; however, as already mentioned, some of these assumptions are not reasonable and deviate from the actual EAF conditions, but are applied to calculations to provide the same EAF conditions or the results cannot be compared. The data from other papers that was needed for validation was extracted with a suitable software (Plot Digitizer).[23]

The first validation of the presented model is done by comparing the obtained results with the study performed by Li et al.[11] who studied a change of mass of a square bar with different sizes melting in the EAF. Steel bars of 170 mm height were positioned vertically (one at the time) in the EAF with forced velocity field established by the coils around the furnace. Afterward, a change of mass of the bars was obtained and the measurements are compared with the results of the model proposed in this paper, using the same steel shape, size, and other EAF conditions, in **Figure 5**. The change of mass was simulated using Equation 11 and the HTC calculation using Equation 18 implemented in a comprehensive EAF model as shown in Figure 1.

As can be seen in Figure 5, in reality (measured data) a slight solidification of the steel occurs around the bar immediately after submerging it in the bath, i.e. current mass (M) of the bar being higher than its initial mass ($M0$). Since the model presented, describes the solidification around the bar with simplified equations, the results are slightly different when compared to the measured data. Otherwise, observing the measured and model-simulated results for the melting period, it can be seen that estimation of the model accurately follows the actual melting of the steel bars, which proves the accuracy of the estimated HTC for the given case.

The second validation of the presented model is done by comparing the results with the most up-to-date studies in this area, i.e., Arzpeyma et al. works[8,16] who studied the

Property	Value
Steel density (kg m^{-3})	6900
Steel specific heat capacity (J (kg K)$^{-1}$)	792
Steel viscosity (kg (m s)$^{-1}$)	0.007
Steel thermal conductivity (W (m K)$^{-1}$)	35
Steel thermal expansion (1 K^{-1})	0.0003
Steel latent heat of fusion (kJ kg^{-1})	240
Scrap radius (m)	0.15

Table 1. Governing conditions as assumed by Arzpeyma et al.[8]

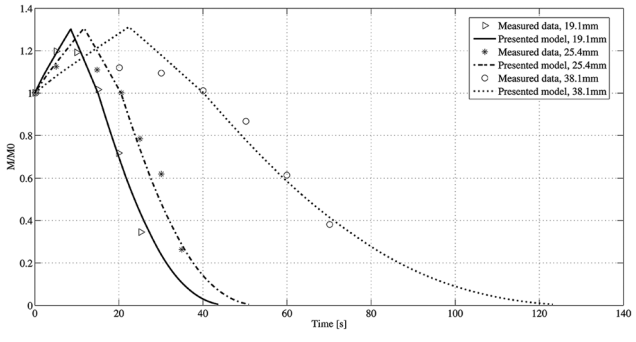

Figure 5. Comparison between the measured[11] and the simulated melting curves for steel bars of different sizes

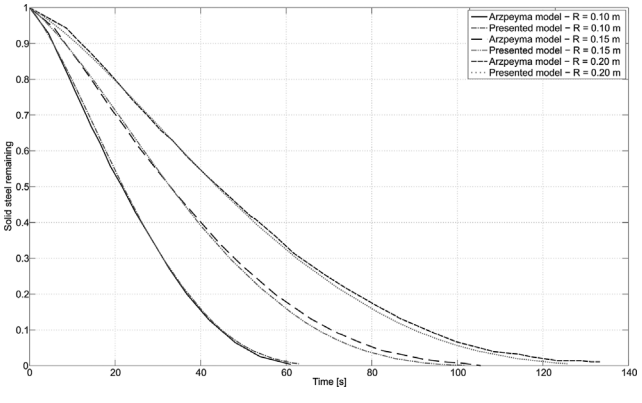

Figure 6. Comparison between the measured[8] and the simulated melting curves for steel cylinders with different radiuses and 0.14 m height for bath velocity of 0.225 m s^{-1}

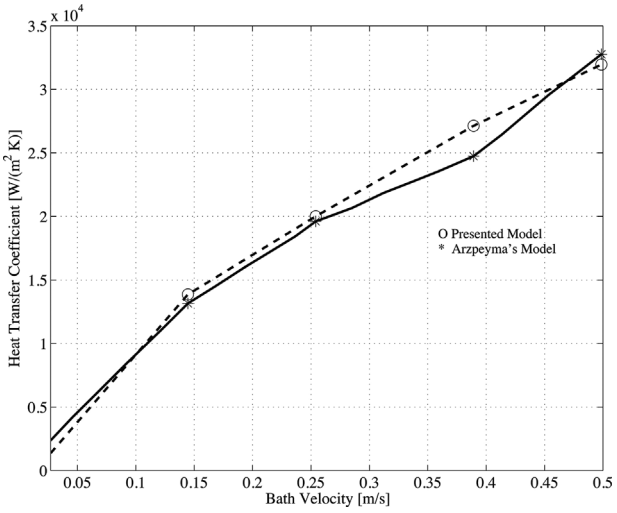

Figure 7. Comparison between the measured[16] and the simulated average HTCs for different bath velocities.

effect of different bath velocities and steel–cylinder radiuses on the HTC. First, a comparison between the work of Arzpeyma et al.[8] and the presented model for different radiuses of the cylinders is obtained. Volumes of the cylinders have been used to calculate the dimensions of the cuboids in the presented model. The parameters in the model assume equal governing conditions as in the Arzpeyma's works, shown in **Table 1**.

Figure 6 shows the solid steel melting curves for three different steel–cylinder radiuses, i.e., 0.1, 0.15, and 0.2 m and a height of 0.14 m for bath speed of 0.225 $\frac{m}{s}$ as obtained by Arzpeyma et al.[8] and as estimated by the presented model. The change of mass was simulated using Equation 11 and the HTC calculation using Equation 18 implemented in a comprehensive EAF model as shown in Figure 1.

As can be seen in Figure 6, the results are very similar to the results presented by Arzpeyma et al.,[8] which further proves the accuracy of the estimated HTC for the given case. In contrast to the model developed by Arzpeyma et al.,[8] which uses CFD to obtain the results, the presented approach is based on ordinary differential equations and although, the work of Arzpeyma et al.[8] does not mention computational times in the works, it can be assumed that obtaining accurate results with CFD approach, significantly longer computational times are needed in comparison to the approach presented here. The model as presented here takes only 0.25 s to simulate the complete melting of one steel bar using Intel Core i7-4710MQ CPU, 3.5 GHz with 8 GB RAM and SSD drive.

Second, a comparison between the HTC's of Arzpeyma et al.[16] and the HTC proposed (Equation 18) for different bath velocities is obtained and is shown in **Figure 7**.

As can be seen in Figure 7, the results obtained by the proposed approach and the results reported by Arzpeyma[16] are comparable, which is proved by maximum error percentage between the results, being approximately 9.6% at approximately 0.375 m s^{-1} bath velocity.

The presented HTC calculation has further been validated by using a comprehensive EAF model as schematically shown in Figure 1. The obtained simulation results are compared to the measured operational data of a 105 ton EAF. The operational data for two different batches are presented in **Table 2** and **Figure 8**. Table 2 shows the discrete inputs and Figure 2 represents the continuous

Type	Scrap	Fat coke	Lime	Dolomite	Dust	Dolomite	Lime	Lime
Batch (a)								
Injection time [s]	0	0	0	0	0	658	709	761
Mass [kg]	45 900	1014	1080	1010	1437	460	500	520
Type	Dolomite	Scrap	Scrap	FeMn				
Injection time [s]	800	965	1750	3029				
Mass [kg]	490	38279	18500	166				
Batch (b)								
Injection time [s]	0	0	0	0	694	745	786	826
Mass [kg]	46418	699	1070	1000	510	510	510	520
Type	Scrap	Dolomite	Dolomite	Dolomite	Scrap	Al	SiMn	FeSi
Injection time [s]	920	1531	1560	1613	1700	3038	3038	3038
Mass [kg]	36 057	480	480	490	21 993	131	1218	196

Table 2. Discrete inputs for two validation batches.

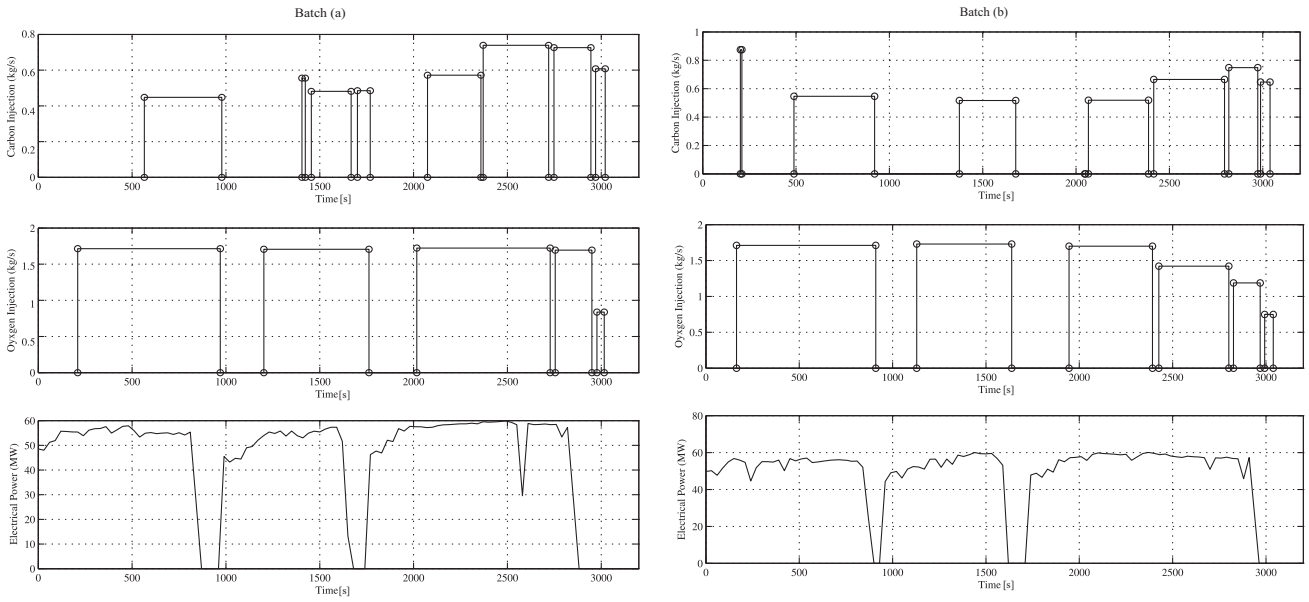

Figure 8. Continuous inputs for two validation batches.

inputs to the EAF. Since the estimation of the HTC has a direct effect on the bath temperature, **Figure 9** and **Table 3** are intended to visualize the difference between the model-simulated and the measured bath temperatures.

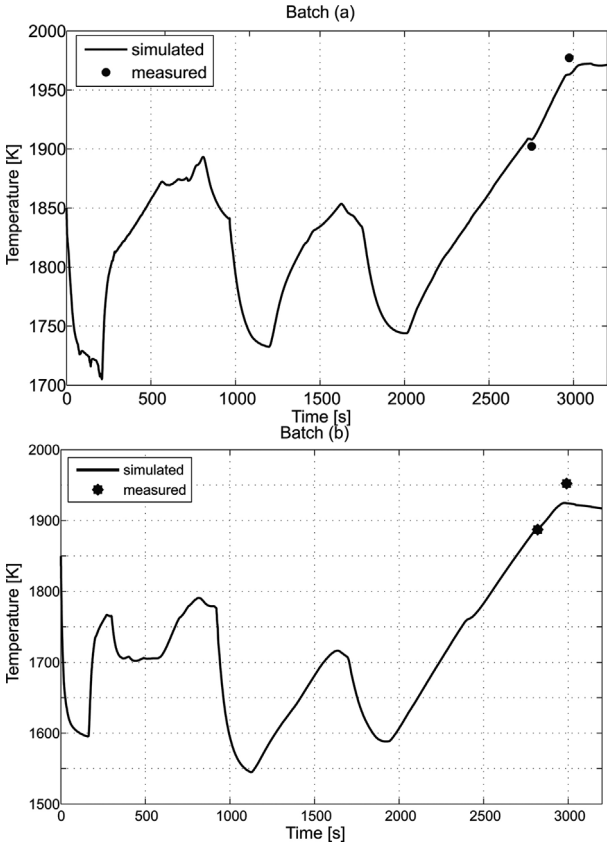

Figure 9. Comparison between the measured and the simulated bath temperatures for two different melting batches.

As shown in Figure 9 and Table 3, the estimated bath temperatures are very close to the measured endpoint bath temperatures. Observing the second measurement of the second batch, a slightly larger deviation from the simulated value occurs, which is most likely a consequence of the EAF sampling-point selection and non-homogenous bath, as the total energy input between the samples (2819 and 2990 s) is too low in order to increase the bath temperature from 1887 to 1952 K. Knowing that temperature gradients in the non-stirred EAF bath can reach up to 80–120 K,[19] the difference between the measured and the simulated temperatures is acceptable. The similarity of the simulated results with the measured EAF data, especially in the prediction of the bath temperature, denotes the accuracy of the presented HTC model. One of the main factors that leads to high accuracy of the model is the implementation of the HTC calculation method as presented in this paper.

5. Conclusion

This paper introduces a model with low computational demand, taking into the account real EAF conditions

	Batch (a)		Batch (b)	
Time [s]	2752	2974	2819	2990
Measured temperature [K]	1902	1977	1887	1952
Simulated temperature [K]	1908	1963	1889	1925

Table 3. Comparison between the measured and the simulated bath temperatures for two validation batches.

and yielding realistic results. Even though the presented model is mathematically simplified and has the advantage of short computational times, the accuracy of estimation is not compromised in comparison to the models running sophisticated CFD software. As has been shown, the results obtained by the model, using equal conditions as the literature review papers, are comparable with the measured data and theoretical models based on partial differential equations. For this reason, the proposed model and the equations originated by the model can be used in broader EAF models and model-based EAF control, where computational times need to be kept as low as possible in order to ensure the real-time operation of the complete system.

6. List of Symbols

Gr	Grashof number
Pr	Prandtl number
Nu	Nusselt number
Re	Reynolds number
Sc	Schmidt number
Sh	Sherwood number
h	heat transfer coefficient (HTC) $\left[\frac{\mathrm{w}}{\mathrm{m^2K}}\right]$
T_{lSc}	liquid steel temperature [K]
T_{sSc}	solid scrap temperature [K]
$T_{\mathrm{sSc_0}}$	initial scrap temperature [K]
T_{m}	melting temperature [K]
T	temperature [K]
ρ_{sSc}	density of the solid steel
ΔH_{f}	latent heat of fusion
ϑ	moving velocity of the interface $\left[\frac{\mathrm{m}}{\mathrm{s}}\right]$
k_{sSc}	thermal conductivity of the solid steel $\left[\frac{\mathrm{w}}{\mathrm{mk}}\right]$
C_{PsSc}	specific heat of the solid steel $\left[\frac{\mathrm{J}}{\mathrm{kgK}}\right]$
C_{PlSc}	specific heat of the liquid steel $\left[\frac{\mathrm{J}}{\mathrm{kgK}}\right]$
$h_{\mathrm{motionless}}$	HTC in motionless interface $\left[\frac{W}{m^2K}\right]$
k_{sSc}	liquid steel thermal conductivity $\left[\frac{\mathrm{w}}{\mathrm{mk}}\right]$
L_{C}	characteristic length [m]
$Q_{\mathrm{lSc-sSc}}$	power transferred from liquid to solid steel
A	solid area covered by liquid steel [$\mathrm{m^2}$]
Q_{sSc}	net power input to solid scrap zone
m_{sSc}	solid scrap mass [kg]
L_{P}	length of the flow path [m]
H, W, L	height, width and length of the cuboid [m]
V_{lSc}	bath velocity $\left[\frac{\mathrm{m}}{\mathrm{s}}\right]$
μ	dynamic viscosity $\left[\frac{\mathrm{Ns}}{\mathrm{m^2}}\right]$
t_{melting}	time needed to melt the scrap [s]
$L_{\mathrm{sSc_0}}$	initial length of the cuboid-shaped scrap [m]
DMT	decrease of the melting time due to liquid steel temperature %
C_{SL}	dimensionless coefficient representing the effect of the solid scrap placement in the bath
$M0$	initial solid part mass
M	current solid part mass

7. List of Common Sub Indexes

sSc solid steel
lSc liquid steel

Received: February 23, 2015;
Published online: September 7, 2015

Keywords: EAF; heat transfer coefficient; melting rate; stirring; velocity distribution

References

[1] Y. N. Toulouevski, I. Y. Zinurov, *Innovation in Electric Arc Furnaces*, Springer, Germany **2009**.
[2] *A Handbook of World Steel Statistics*, International Iron and Steel Institute, Belgium **1978**.
[3] *World Steel in Figures 2012*, World Steel Association, Belgium **2012**.
[4] R. J. Fruehan, A. S. Foundation, *The Making, Shaping, and Treating of Steel*, The AISE Steel Foundation, USA **1999**.
[5] J. G. Bekker, I. K. Craig, P. C. Pistorius, *ISIJ Int.* **1999**, *39*, 23.
[6] V. Logar, D. Dovzan, I. Škrjanc, *ISIJ Int.* **2012**, *52*, 402.
[7] V. Logar, D. Dovzan, I. Škrjanc, *ISIJ Int.* **2012**, *52*, 413.
[8] N. Arzpeyma, O. Widlund, M. Ersson, P. Jönsson, *ISIJ Int.* **2013**, *53*, 48.
[9] R. I. L. Guthrie, L. Gourtsoyannis, *Can. Metal. Q.* **1971**, *10*, 37.
[10] M. Kawakami, K. Takatani, L. C. Brabie, *Tetsu-To-Hagane J.* **1999**, *85*, 658.
[11] J. Li, N. Provatas, G. Brooks, *Metall. Mater. Trans. B* **2005**, *36*, 293.
[12] A. K. Shukla, O. Volkova, P. R. Scheller, B. Deo, *Metall. Mater. Trans. B* **2011**, *42*, 224.
[13] F. Kreith, W. Z. Black, *Basic Heat Transfer*, Harper & Row, USA **1980**.
[14] J. Madias, *Electric Furnace Steelmaking*, Elsevier, USA **2014**.
[15] G. Dressel, *Ironmak Steelmak* **1998**, *25*, 61.
[16] N. Arzpeyma, *Modeling of Electric Arc Furnaces (EAF) with Electromagnetic Stirring*, M. Sc. thesis, Royal Institute of Technology, Sweden **2011**.
[17] L. P. Rathaba, *Model fitting for Electric Arc Furnace Refining*, University of Pretoria, South Africa **2005**.
[18] S. Paik, H. D. Nguyen, *Int. J. Heat Mass Transfer* **1995**, *38*, 1161.
[19] O. J. P. Gonzalez, M. Ramírez-Argáez, A. N. Conejo, *ISIJ Int.* **2010**, *50*, 1.
[20] A. K. Shukla, B. Deo, D. Robertson, *Metall. Mater. Trans. B* **2013**, *44*, 1407.
[21] J. R. Culham, M. M. Yovanovich, P. Teertstra, C.-S. Wang, G. Refai-Ahmed, R. Tain, *J. Electron. Packag.* **2001**, *123*, 7.
[22] S. Lee, M. M. Yovanovich, K. Jafarpur, *J. Thermophys.* **1991**, *5*, 208.
[23] J. Huwaldt, PLOT DIGITIZER 2.5.0., http://plotdigitizer.sourceforge.net, **2010**.